Scenario Characteristics Driven Maritime VHF Spectrum Measurement and Channel Occupancy Modeling

Chensong Zhao, Qing Hu, Yanpeng Dai, *Member, IEEE*, Chang Liu, Shuaiheng Huai, *Member, IEEE*, Nan Cheng, *Senior Member, IEEE*, and Xuemin Shen, *Fellow, IEEE*

***Abstract*—Maritime Very High Frequency (VHF) band supports essential maritime applications such as radiotelephony (RT) and Automatic Identification System (AIS). Catering to the advance of broadband and digital maritime communications, empirical measurement and modeling of maritime VHF band become crucial steps. In this paper, we conduct a continuous seven-day (24/7) measurement in the Laotieshan VTS coverage waters (Dalian, China), to collect synchronized RF and AIS data. We then fit multiple candidate probability distributions to the observed occupancy patterns and develop lognormal and generalized Pareto distributions models for the ON/OFF sojourn time of active VHF RT and AIS channels, providing substantial opportunities for spectrum reuse. Furthermore, we introduce a set of scenario characteristics, and analyze their correlations with channel occupancy. Based on multiple linear regression, we develop a scenario-driven time-series generation model (SD-model) for maritime VHF RT channels. Simulation results show that the SD-model is accurate for the occupancy and ON/OFF sojourn time distributions of active VHF RT channels, and therefore for validating spectrum access techniques in the maritime VHF band.**

***Index Terms*—Spectrum usage models, maritime communications, very high frequency(VHF), spectrum management.**

I. Introduction

THE Very High Frequency (VHF) band, allocated at 156.025-162.025 MHz, is the primary spectrum for global maritime communications, supporting VHF radiotelephony (RT) and Automatic Identification System (AIS) maritime applications, and it is critical for safe and efficient maritime navigation [1]. Existing maritime communication systems are increasingly unable to satisfy the digitized demand of marine users for higher bandwidth, lower latency, and lower costs [2]. The U.S. maritime administration indicated that peak AIS data link loading exceeds 64% [3], presenting significant risks to navigational safety. VHF RT as the primary means of communication for port ship scheduling, occupies much of the maritime VHF band allocation. However, it still relies on manual channel selection and FM modulation voice calls, resulting in low communication efficiency and spectrum waste, which means the transformation of digital technology is urgent. Therefore, measurement and modeling the maritime VHF channel usage patterns, and providing available spectrum resources are significant toward the digitalization of maritime communications.

Maritime VHF channel usage patterns are closely related to local scenario characteristics. Ship density is a potential factor of VHF RT load. Higher density implies busier traffic flows and more frequent VHF RT calls for supporting port operations. However, the effects of scenario characteristics on channel usage patterns are not uniform, even the same characteristic may influence patterns differently across sea areas. Therefore, the maritime scenario oriented for VHF spectrum measurement and channel occupancy modeling methodology is necessary to analyze the scenario characteristics correlations, providing a solid theoretical basis for the digital transformation of the maritime VHF band.

There exist several studies on maritime channel measurement. Mi et al. [4] conducted a wireless channel sounding campaign in a land-to-ship scenario at 3.2 GHz, and analyzed the wireless channel characteristics in scenarios featuring islands. Lyu et al. [5] reported a fixed-to-fixed, beyond the horizon measurement campaign at 25 GHz, examining mmWave path loss via evaporation ducting. Zhang et al. [6] presented maritime propagation measurements at 8 GHz in the South China Sea and fitted the fading statistics with multiple distribution models. Brennan et al. [7] studied propagation for ad hoc 2.4/5 GHz WLAN systems used near shore for autonomous surface vehicles. Li and Wang et al. [8], [9] investigated radio characteristics and propagation models for vessel communications in the Pearl River estuary and inland ports. Lee et al. [10] reported

Received 23 December 2025; revised 26 February 2026; accepted 24 March 2026. Date of publication 30 March 2026; date of current version 17 August 2026. This work was supported in part by the National Natural Science Foundation of China under Grant 62571081, in part by the Key Research and Development Program of Liaoning Province under Grant 2025JH2/102700003, in part by the Fundamental Research Funds for the Central Universities under Grant 3132025805, and in part by Liaoning Provincial Science and Technology Joint Plan under Grant 2025-MSLH-061 and Grant 2025-MSLH-055. The review of this article was coordinated by Dr. Shaowei Wang. *(Corresponding author: Qing Hu.)*

Chensong Zhao, Qing Hu, Yanpeng Dai, Chang Liu, and Shuaiheng Huai are with the School of Information Science and Technology, Dalian Maritime University, Dalian 116026, China, and also with the National Engineering Research Center of Maritime Navigation System, Dalian Maritime University, Dalian 116026, China (e-mail: zhaochensong@dlmu.edu.cn; hq0518@dlmu.edu.cn; yanpengdai@dlmu.edu.cn; liuchang@dlmu.edu.cn; huaishuaiheng@dlmu.edu.cn).

Nan Cheng is with the State Key Laboratory of Integrated Services Networks and the School of Telecommunications Engineering, Xidian University, Xi'an 710071, China (e-mail: dr.nan.cheng@ieee.org).

Xuemin Shen is with the Department of Electrical and Computer Engineering, University of Waterloo, Waterloo, ON N2L 3G1, Canada (e-mail: sshen@uwaterloo.ca).

Digital Object Identifier 10.1109/TVT.2026.3678658

land-to-ship offshore measurements using a narrowband system between a quay and a patrol boat. Hui et al. [11] investigated line-of-sight radiowave propagation near the sea surface at 5 GHz using narrowband measurements. Studies [4], [5], [6], [7], [11] address channel modeling in maritime millimeter-wave (mmWave) bands, whereas [8], [9], [10] focus on maritime channel modeling in specific port environments. Although these studies provide comprehensive measurements span open-sea, inland-waterway, and island environments. Nevertheless, the emphasis has been channel modeling, with little work on channel occupancy modeling and availability analysis for the maritime VHF band.

There exist several studies on spectrum occupancy modeling. Haralambous et al. [12], [13] used neural networks and nonlinear regression to model HF spectrum allocation. Mostafa et al. [14] used time-series techniques to characterized HF occupancy in the Eastern Mediterranean. Barnes et al. [15] measured TV white space (TVWS) at six sites on the University of Pretoria's Hatfield Campus and reported multiple white space opportunities. Corral-De-Witt et al. [16] measured the 500-698 MHz UHF-TV band in Windsor, Canada, and proposed a probabilistic model to identify TVWS. Rutagemwa et al. [17] examined shared spectrum scenarios in the land mobile radio (LMR) bands using a spectrum monitoring system in Ottawa, Canada. López et al. [18] proposed a two-state discrete-time Markov chain with novel deterministic and stochastic duty cycle models for spectrum access validation studies. López et al. [19] sampled several common bands fitting multiple stochastic processes and proposing a model that captures statistical behavior at both low and high time resolutions. In a separate study, López et al. [20] collected multi-band measurements in urban buildings and introduced a spatial modeling method. Palaios et al. [21] analyzed spectrum usage and radio environment dynamics based on measurement campaigns in the metropolitan areas of Paris and London. Wang et al. [22] surveyed three public spectrum databases about measurement result. Chen et al. [23] reviewed occupancy models derived from campaigns up to 2013 and discussed techniques for extracting complete statistical models from raw measurements. Höyhtyä et al. [24] surveyed occupancy across time, space, frequency, and power domains, and emphasizing the decisive role of measurement location. Das et al. [25] compared worldwide occupancy models and synthesized empirical findings across scenarios, with particular attention to the fraction of spectrum used by different applications. Dinesh et al. [26] proposed a generic spectrum-surveying framework for the collection, analysis, and modeling of spectrum measurements. [27] and [28] analyzed spectrum occupancy models using different machine learning based enhancement methods. Measurement and modeling of the VHF band are the first steps toward analyzing maritime channel availability. However, the aforementioned studies statistically model spectrum occupancy across multiple frequency bands and locations, but they do not address the VHF band.

In addition, measurement and occupancy modeling for the VHF band or maritime settings have also been studied. Hu et al. [29] measured VHF voice communication occupancy at Guangzhou's Hancheng Airport, China, finding utilization below 22% and highlighting substantial opportunities for spectrum reuse. Loquias et al. [30] evaluated spectrum activity in the 470-698 MHz UHF band over Philippine waters and confirmed available white space opportunities along maritime routes. Hashim et al. [31] present an experimental quantitative analysis of the dynamic behavior of VHF at 174-230 MHz band in Malaysia land, which result shows a low utilization of the VHF band. In summary, although extensive spectrum availability analyses have been conducted across various scenarios and frequency bands, dedicated studies on spectrum occupancy modeling for the maritime VHF band remain markedly insufficient, hindering the advancement of maritime communications digitalization.

In this paper, we conduct a seven-day measurement campaign of maritime VHF signals, capturing both RF emissions and AIS reports. We analyze the occupancy patterns of maritime VHF applications within specific channels, fit candidate probability distributions to the measured ON/OFF sojourn times of active VHF RT and AIS channels, and using AIS-derived geospatial information, introduce a set of scenario characteristics to quantify environmental and traffic conditions. We then perform correlation analysis and develop a scenario-driven time-series generation model (SD-model) for maritime VHF RT channels. The proposed approach can simulate ON/OFF sojourn times of VHF RT channels and supports model development for other busy waterways and ports. The main contributions are as follows:

1) We conduct a continuous, seven-day field measurement campaign in the Laotieshan water, Dalian, China, collecting synchronized VHF RT and AIS data to quantify correlations between in situ scenario characteristics and voice-call application load. To the best of our knowledge, this is the first study to jointly analyze AIS-derived data and maritime VHF RT channel occupancy.
2) We analyze several candidate probability distributions to the measured data and present a distributional model of ON/OFF state durations for VHF RT and AIS channels.
3) We develop a SD-model for maritime VHF RT channels. Specifically, we introduce a set of scenario characteristics (e.g., ship density) and conduct linear-regression-based correlation analyses between these characteristics and channel occupancy. We then analyze the impact of the scenario characteristics on arrival intensity using a nonhomogeneous Poisson process (NHPP) and present a SD-model for maritime VHF RT channels.

The rest of this paper is organized as follows. Section II describes the measurement setup, how occupancy is calculated, and presents observational results. Section III explains the fitting of distribution models for active channels and shows the results. Section IV introduces the definition of scenario characteristics and the SD-model for maritime VHF RT channels. Section V reports the correlation analysis and compares the SD-model with the measured data. Section VI concludes this paper.

II. Measurement Campaign and Channel Occupancy Statistics

In this section, we first describe the measurement scenario, then detail the measurement system and procedure, and finally

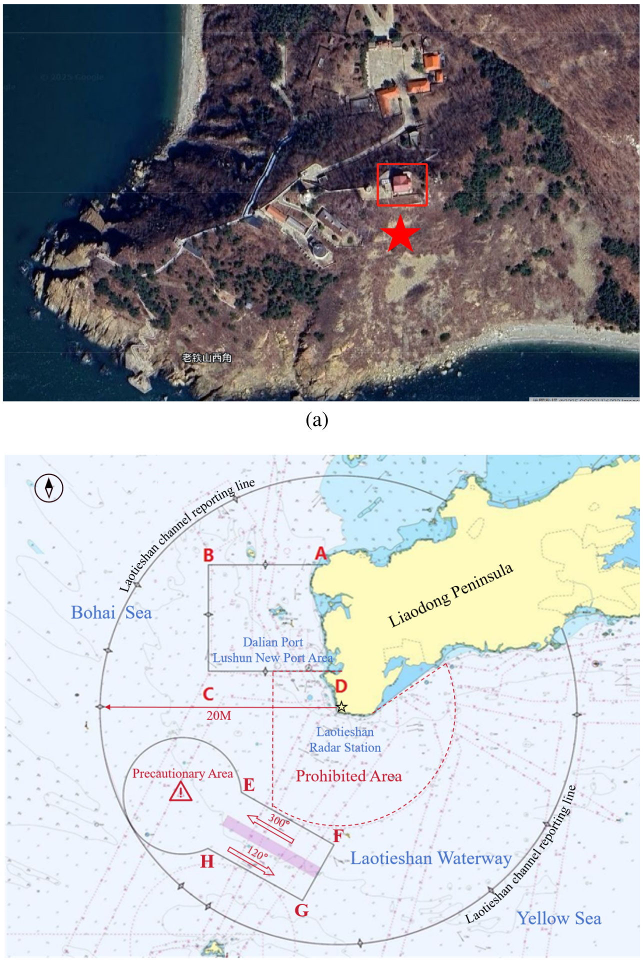

(a)

(b)

Fig. 1. Overview of the measurement site and nearby sea regions. (a) Laotieshan Lighthouse Monitoring Station, Dalian Maritime Buoy Service Center. (b) Laotieshan VTS Area.

present the methodology and results for quantifying channel occupancy on active VHF channels.

A. Measurement Environment

As shown in Fig. 1(a), we conducted maritime VHF channel measurement at the lighthouse monitoring station of Laotieshan, Dalian Maritime Buoy Service Center, Dalian, China. The measurement site is near the hydrological boundary between the Yellow Sea and the Bohai Sea at 38°43′37″ N, 121°8′2″ E, with an elevation of about 100 meters. The vantage point is surrounded by open sea on three sides with no obstructions, allowing for high quality reception of VHF signal across the Laotieshan waters.

The waters surrounding the Laotieshan Lighthouse monitoring station (hereinafter, the Laotieshan VTS area) form a principal waterway linking the Yellow Sea and the Bohai Sea. With substantial shipping traffic and active communications, this area is an ideal field site for maritime VHF band channel measurements. Specifically, as shown in Fig. 1(b), this area is

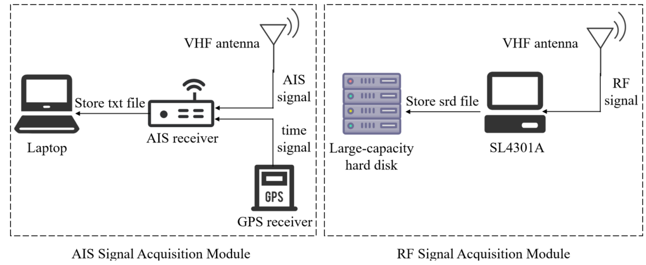

Fig. 2. Measurement workflow.

(a) SL4301A RF receiver

(b) AIS signal receiver

Fig. 3. Signal acquisition equipment.

defined as the waters within a 20 nautical miles radius centered on the Laotieshan Lighthouse, principally encompassing the Lvshun New Port VTS sector and the Traffic Separation Scheme (TSS). The Lushun New Port VTS sector covers the area bounded by points A (38°56′00″ N, 121°06′30″ E), B (38°56′00″ N, 120°54′00″ E), C (38°47′07″ N, 120°54′00″ E), and D (38°47′07″ N, 121°08′25″ E), connected sequentially to the coastline, with the connecting segments constituting reporting lines. The TSS covers the precautionary area with a radius of 5 nautical miles centered at 38°36′24″ N, 120°51′18″ E, as well as the divided traffic separation scheme area bounded by points E (38°36′42″ N, 120°57′36″ E), F (38°32′12″ N, 121°07′36″ E), G (38°27′30″ N, 121°04′06″ E), and H (38°31′54″ N, 120°54′06″ E), connected in order. All foreign ships and Chinese A-class ships transiting the reporting line must submit voice reports to the Laotieshan VTS on VHF RT channel 10 (VHF 10). The report shall include basic information such as ship name, call sign, draft, speed, course and destination. In addition, ships operating within the Laotieshan VTS area shall maintain a continuous watch on VHF 10 and VHF RT channel 16 (VHF 16), and comply with VTS navigational instructions [32].

B. Measurement Setup

We synchronously collect VHF RF signals and AIS signals. The RF data are used to analyze per-channel usage patterns (e.g., active channels VHF 10/16), while the AIS data are decoded to obtain ship trajectories for subsequent joint analysis. As shown in Fig. 2, the measurement workflow comprises two modules: an RF signal reception module and an AIS signal reception module. The RF module continuously acquires and stores maritime VHF band signals. The receiver is the SL4301 A RF signal acquisition/record/playback instrument (Zhongxing Lianhua, as shown in Fig. 3(a)). It is connected to the VHF antenna through an 8 dB attenuator and stores the captured baseband I/Q data as 16-bit integers in SRD files. The sampling volume is approximately

TABLE I
SAMPLING SCHEME

Type	Parameter
Sampling Frequency	12.5 MHz
Intermediate Frequency	159.025 MHz
Sampling Bandwidth	8 MHz
Measurement Start Time	2025-06-12 18:00
Sampling Duration	about 7 days
Single Sample Duration	1 min

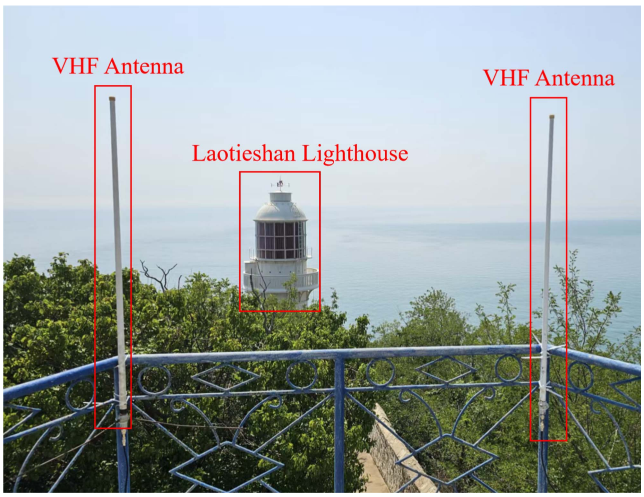

Fig. 4. Antenna installation site.

2.78 GB per minute. Data are offloaded every 24 hours to a 30 TB high capacity hard drive, ensuring uninterrupted acquisition for communication applications in the maritime VHF band. The basic acquisition parameters are summarized in Table I.

The AIS reception module collects and stores ship trajectory information for the Laotieshan VTS area, as shown in Fig. 3(b). The AIS equipment receives AIS signals via a VHF antenna and uses a GPS receiver for precise time synchronization. Real-time AIS data are recorded through a USB serial connection to a laptop in. txt format for subsequent decoding ship trajectories. Meanwhile, two VHF omnidirectional antennas were installed on a rooftop at roughly the same elevation as the lighthouse (as Fig. 4 shows the center red box marks the lighthouse), facing the open sea and connecting to the two reception modules to ensure stable signal reception. Long duration, continuous acquisition yields large volumes of VHF band baseband I/Q data along with AIS-derived ship tracks, providing the observational basis for the analysis methods presented below.

C. Measurement Results and Channel Occupancy Statistics

1) Measurement Results: Fig. 5 illustrates the measured spectrogram of the maritime VHF band for 12 hours. As shown in Fig. 5, calling activity on VHF 10 is noticeably more frequent than on VHF 16, and AIS 1 and AIS 2 transmit data using TDMA. The center frequencies of VHF 10/16 and AIS 1/2 are 156.5, 156.8, 161.975, and 162.025 MHz respectively. During this time, little communication activity is observed on the other channels, that indicates significant spectrum reuse opportunities. Fig. 6 illustrates AIS-derived ship tracks for 1 h, showing that most ships entering or leaving the Bohai Sea via the Yellow Sea transit this corridor, confirming Laotieshan water as a busy navigation area.

2) Channel Occupancy Statistics: The VHF RT and AIS are predominant maritime applications over maritime VHF band within Laotieshan VTS area. We follow the "80% method" in ITU-R SM.1753 [33] to determine the noise power used for ON/OFF state decisions to quantify maritime channel occupancy in the VHF band. Suppose there are L channels, each channel yields M_l power samples denoted by p_{l,m_l} during the observation time. Sorting all samples in ascending order to obtain the sequence $\{p_1 \leq p_2 \leq \cdots \leq p_M\}$, where $M = M_l \times L$. Let $A = \lfloor 0.2M \rfloor$. Then the estimated noise power threshold is given by

$$\hat{P}_{\text{noise}} = \frac{1}{A} \sum_{m=1}^{A} p_m. \tag{1}$$

Meanwhile, we follow ITU-R SM.2256-1 [34] to calculate the frequency channel occupancy rate (FCO) and spectrum resource occupancy rate (SRO). Note that the instantaneous channel state can only be busy (ON state) or idle (OFF state), and the occupancy rate must be averaged over the integration time t. Thus, the l-th channel FCO is given by

$$FCO = \frac{t_s \sum_{m_l=1}^{M_l} I\left(p_{l,m_l} > \hat{P}_{\text{noise}}\right)}{t}, \tag{2}$$

where t_s denotes sample interval. $I(\cdot)$ is the indicator function, which equals 1 if the condition $(\cdot)$ is met and 0 otherwise. SRO represents the overall occupancy ratio of time-frequency resources. Then, the SRO is given by

$$SRO = \frac{\sum_{l=1}^{L} \sum_{m_l=1}^{M_l} I\left(p_{l,m_l} > \hat{P}_{\text{noise}}\right)}{M}. \tag{3}$$

Fig. 7 illustrates the occupancy histogram for all channels in the maritime VHF band. Over the seven-day observation period, the four channels VHF 10/16 and AIS 1/2 are active, handling most maritime communications, with VHF 10 showing more frequent activity than VHF 16. Additionally, beyond these active channels, several other channels also carry some ship-to-ship communications, but their share over the seven days remains low.

Fig. 8 illustrates the time series for the four active channels and the SRO metric with a 1 h integration time. The occupancy rates of AIS 1/2 stay consistently between 5–10% . This indicates that, at the current stage, the AIS system capacity in the Laotieshan waters has not yet reached saturation. Overall, VHF 10 has a significantly higher occupancy than VHF 16, and the peak occupancies of VHF 10 and VHF 16 exceed 20% and 12% , respectively, with noticeable variability in the curves. This variability occurs because VHF RT channel occupancy is closely connected to scenario characteristics such as ship density, traffic control, and on-site dispatching. Lastly, the SRO for the entire band remains steadily low over the seven-day measurement period, around 1–2% . These findings show that the

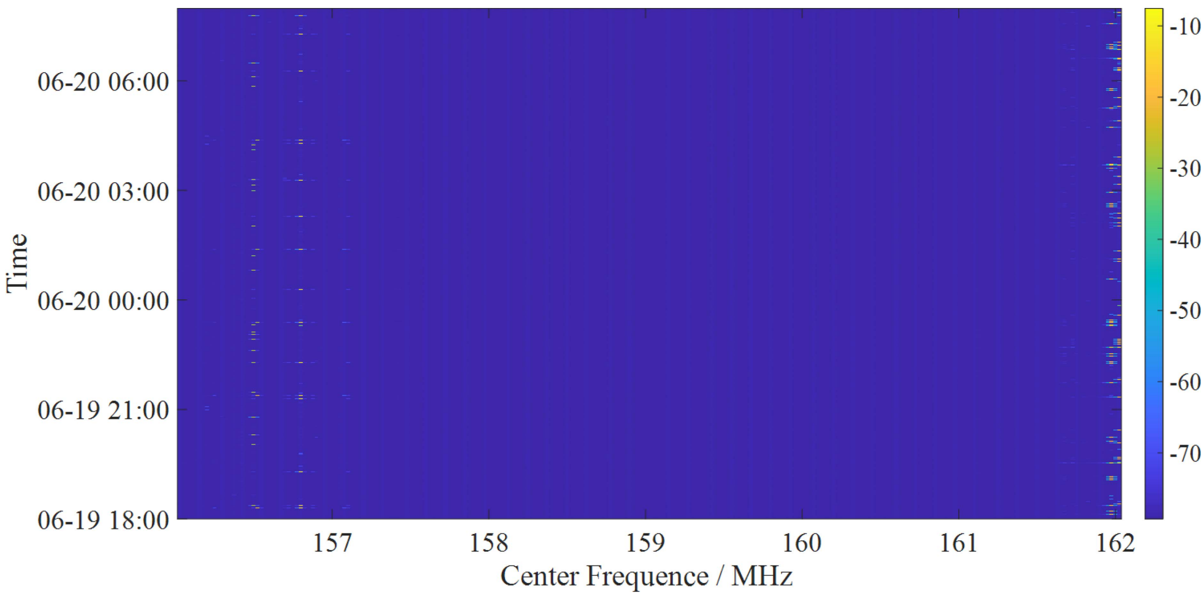

Fig. 5. Spectrogram of the maritime VHF band.

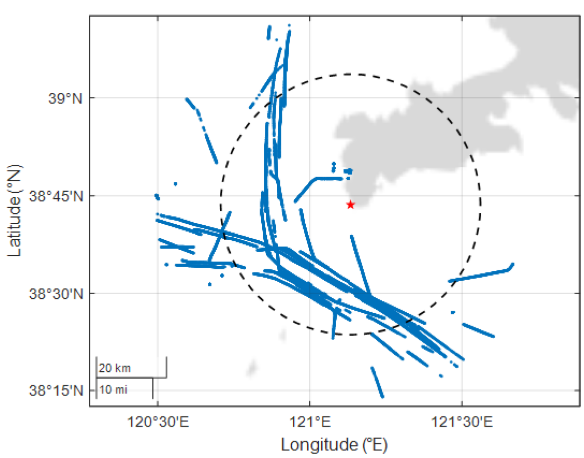

Fig. 6. Ship trajectories on June 12, 2025, from 6:00 PM to 7:00 PM (local time).

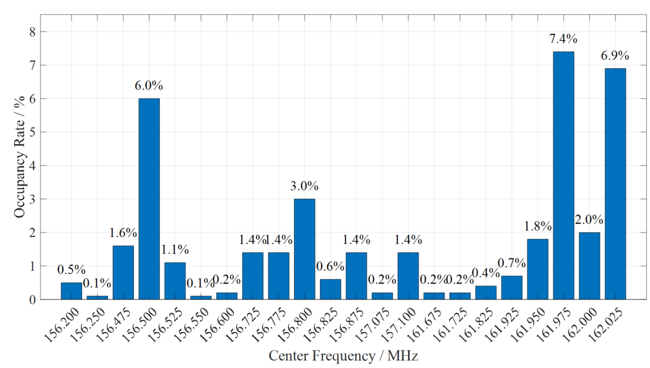

Fig. 7. FCO for all channels during the seven-day observation period.

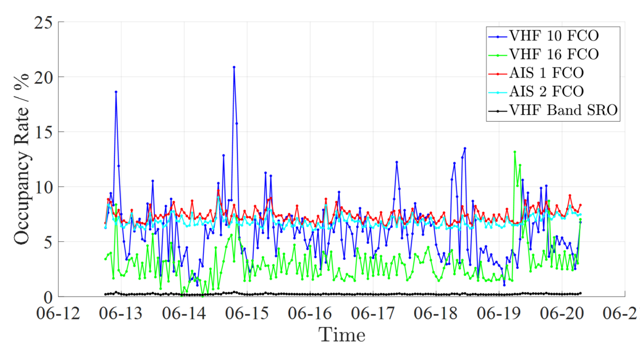

Fig. 8. FCO/SRO of active channels during the seven-day observation period.

spectrum utilization of current VHF RT communications is low, leaving ample space for spectrum reuse and providing a solid basis for gradually adopting maritime digital communication technologies.

III. Probabilistic Fitting of Channel Occupancy Model

A. *Selected Probability Models and GOF Metrics*

Fitting the collected data with probability distributions from stochastic process theory enables analysis of real signal occupancy patterns and provides statistical characteristics of PU spectrum usage for cognitive radio systems. Based on the two-state ON/OFF time series extracted from the measurements, we derive empirical cumulative distribution function (CDF) for the four active channels and compare them against candidate distributions to characterize the probabilistic model of VHF channels.

The simple distributions considered include the exponential (EX), generalized exponential (GE), generalized Pareto (GP), lognormal (LN), gamma (GM), and Weibull (WB) models. The EX distribution has been widely used to describe state residence times in continuous time Markov chains (CTMC).

However, numerous studies have shown that wireless traffic often exhibits pronounced heavy tails, making the exponential model inadequate in practice. The LN distribution has been recommended for heavy tailed data [35]. The GE distribution provides strong versatility by replicating other shapes through its shape parameters. The GP distribution effectively captures channel occupancy durations [19], and the GM and WB distributions are likewise widely used to model occupancy patterns in operational communication systems.

We estimate distribution parameters from the collected data using maximum likelihood estimation (MLE). To evaluate the appropriateness of the fits, we use three goodness-of-fit (GOF) metrics: Kolmogorov-Smirnov (KS) distance, Kullback-Leibler (KL) divergence [36], and Bhattacharyya distance [37]. These GOF measures numerically assess how well each parametric distribution matches the empirical durations of the ON/OFF states.

The KS distance D_{KS} denotes the difference between the CDF $F_{\text{fit}}(\mathcal{T}_{\text{s}})$ of the ON or OFF period time and the empirical CDF $F_{\text{emp}}(\mathcal{T}_{\text{s}})$, where $\mathcal{T}_{\text{s}}$ represents the ON/OFF state stay time, the equation is as follows

$$D_{\text{KS}} = \max_{\mathcal{T}_{\text{s}}} \left\{ \left| F_{\text{fit}}\left(\mathcal{T}_{\text{s}}\right) - F_{\text{emp}}\left(\mathcal{T}_{\text{s}}\right) \right| \right\}, \tag{4}$$

Kullback-Leibler (KL) divergence can be given as

$$D_{\text{KL}} = \sum_{t=1}^{T} f_{\text{emp}}(t) \ln\left(\frac{f_{\text{emp}}(t)}{f_{\text{fit}}(t)}\right) + \sum_{t=1}^{T} f_{\text{fit}}(t) \ln\left(\frac{f_{\text{fit}}(t)}{f_{\text{emp}}(t)}\right), \tag{5}$$

where $f_{\text{emp}}(t)$ and $f_{\text{fit}}(t)$ denote the empirical probability density function (PDF) and the evaluated PDF model, respectively. $t = 1, 2, \ldots, T$ denotes the t-th integration time, and T denotes full observation time. The Bhattacharyya distance can be expressed as

$$D_{\text{BD}} = -\ln\left(\sum_{t=1}^{T} \sqrt{f_{\text{emp}}(t) \cdot f_{\text{fit}}(t)}\right). \tag{6}$$

A lower value of the GOF metrics indicates a better fit. A value of zero means that, with the current parameters, the probabilistic model perfectly matches the empirical distribution.

B. Probability Distribution Fitting Results

Using the RF measurement data, we evaluate the suitability of CDF for VHF 10, VHF 16, AIS 1, and AIS 2 in describing ON and OFF durations. Parameters are estimated via MLE, and GOF metrics determine the most appropriate probability distribution for each channel. As shown in Table II, lower values indicate a stronger descriptive ability of a distribution for a channel's ON/OFF durations. The results show that, for the ON duration of VHF 10, the KS distance and KL divergence reach their minimums under the LN model, although the Bhattacharyya distance is not the smallest, its accuracy is only slightly lower than the best GE model, indicating that the LN model is suitable for VHF 10 ON durations. VHF 10 OFF durations show a similar pattern, with the GP model providing the best fit. For VHF 16 ON/OFF durations, the KS distance and KL divergence favor the GP model, and despite a different signal from the Bhattacharyya distance, the voting rule indicates that the GP model is the most appropriate for VHF 16 ON/OFF durations.

TABLE II
THE GOF FITTING RESULTS OF THE FOUR ACTIVE CHANNELS

Channel	GOF	EX	GP	LN	GM	WB	GE
VHF 10	$D_{\text{KS}}^{\text{ON}}$	0.211	0.224	**0.099**	0.113	0.153	0.111
	$D_{\text{KL}}^{\text{ON}}$	0.432	0.436	**0.202**	0.279	0.359	0.248
	$D_{\text{BD}}^{\text{ON}}$	0.053	0.055	0.026	0.025	0.037	**0.022**
	$D_{\text{KS}}^{\text{OFF}}$	0.456	**0.087**	0.119	0.232	0.169	0.239
	$D_{\text{KL}}^{\text{OFF}}$	1.315	**0.212**	0.264	0.609	0.432	0.630
	$D_{\text{BD}}^{\text{OFF}}$	0.168	0.126	**0.124**	0.188	0.168	0.191
VHF 16	$D_{\text{KS}}^{\text{ON}}$	0.321	**0.103**	0.116	0.223	0.175	0.231
	$D_{\text{KL}}^{\text{ON}}$	1.368	**0.630**	0.662	0.989	0.84	1.012
	$D_{\text{BD}}^{\text{ON}}$	0.182	0.107	**0.078**	0.174	0.153	0.178
	$D_{\text{KS}}^{\text{OFF}}$	0.511	**0.112**	0.148	0.220	0.179	0.221
	$D_{\text{KL}}^{\text{OFF}}$	1.808	**0.506**	0.511	0.736	0.603	0.743
	$D_{\text{BD}}^{\text{OFF}}$	**0.235**	0.305	0.239	0.243	0.239	0.244
AIS 1	$D_{\text{KS}}^{\text{ON}}$	0.589	0.578	0.524	0.525	**0.474**	0.564
	$D_{\text{KL}}^{\text{ON}}$	3.653	3.551	2.479	2.605	2.918	**2.154**
	$D_{\text{BD}}^{\text{ON}}$	1.832	1.788	1.280	1.341	1.506	**1.007**
	$D_{\text{KS}}^{\text{OFF}}$	0.099	**0.074**	0.075	0.08	0.087	0.077
	$D_{\text{KL}}^{\text{OFF}}$	0.542	**0.489**	0.555	0.510	0.508	0.511
	$D_{\text{BD}}^{\text{OFF}}$	0.357	0.336	0.347	**0.335**	**0.335**	**0.335**
AIS 2	$D_{\text{KS}}^{\text{ON}}$	0.589	0.58	0.524	0.525	**0.472**	0.564
	$D_{\text{KL}}^{\text{ON}}$	3.419	3.335	2.276	2.41	2.72	**1.96**
	$D_{\text{BD}}^{\text{ON}}$	1.722	1.687	1.193	1.257	1.416	**0.925**
	$D_{\text{KS}}^{\text{OFF}}$	0.12	0.077	0.127	0.087	**0.073**	0.089
	$D_{\text{KL}}^{\text{OFF}}$	0.556	**0.495**	0.615	0.521	0.507	0.525
	$D_{\text{BD}}^{\text{OFF}}$	0.28	0.259	0.279	0.255	**0.252**	0.257

For AIS 1/2 ON durations, the GE distribution performs best in terms of KL divergence and Bhattacharyya distance, while the KS distance favors the WB distribution. The KS values for all candidate models on AIS 1/2 ON duration data are nearly identical, and the GE model's KS performance is moderate compared to others. Thus, using the GE model for AIS ON durations is acceptable. For AIS OFF durations, AIS 1 has the best KS distance and KL divergence with the GP model, and its Bhattacharyya distance is very close to that of the GM distribution. However, AIS 2 indicates a different trend. Numerical comparison reveals that, the GP fit is only slightly worse than the best fit for AIS 2. Since AIS 1/2 carry similar traffic and have comparable communication patterns, the GP model is considered the most appropriate for AIS OFF durations. Table III summarizes the fitted distribution models and their parameters for all four active channels. Fig. 9 illustrates the fitted curves. The VHF 10/16 ON/OFF durations align with the findings above. The empirical AIS OFF durations curves closely follow the GP trend, which is also consistent with the conclusions. By contrast, AIS ON durations display a distinct step like pattern, indicating that most ON periods are short and tightly clustered without a heavy tail, due to the TDMA mechanism in the AIS bands. This suggests that simple one or two-parameter distributions cannot fully capture the usage patterns of AIS ON durations. Therefore, in the following sections, we will focus our analysis

TABLE III
PARAMETER VALUES OF FITTING RESULTS

Channel	State	Model	Parameter values
VHF 10	ON	LN(μ, σ)	1.02, 0.77
VHF 10	OFF	GP(ξ, σ, θ)	1.31, 8.41, 0
VHF 16	ON	GP(ξ, σ, θ)	0.76, 4.41, 0
VHF 16	OFF	GP(ξ, σ, θ)	2.58, 9.09, 0
AIS 1	ON	GE(a, λ)	3505.84, 16.09
AIS 1	OFF	GP(ξ, σ, θ)	−0.32, 9.30, 0
AIS 2	ON	GE(a, λ)	3218.91, 15.92
AIS 2	OFF	GP(ξ, σ, θ)	−0.27, 9.48, 0

on the modelable VHF 10/16 channels, incorporating scenario characteristics.

IV. SCENARIO-DRIVEN TIME-SERIES GENERATION MODEL

Most existing studies focus on the time-frequency dimensions of the channel occupancy model, but the spatial dimension of the measurement site is equally important. In real-world systems, channels within the same band can show significantly different occupancy behaviors depending on location. For the maritime VHF band, which is the main medium for port operations, collision avoidance, and related activities, channel load is naturally linked to scenario characteristics within the site's coverage, such as ship density and traffic flow. Generally, the busier traffic corridor within the measurement area, the more frequent communication activity and the higher VHF occupancy, and vice versa. Therefore, we collected AIS signals alongside VHF RF measurements to decode ship trajectories and used multiple linear regression to model the arrival intensity of an NHPP as a function of six scenario characteristics: ship number, ship density, line-crossing ship density, busy water ship density, busy water ratio, and time of day. Based on this, we introduce a SD-model for the maritime VHF RT channels.

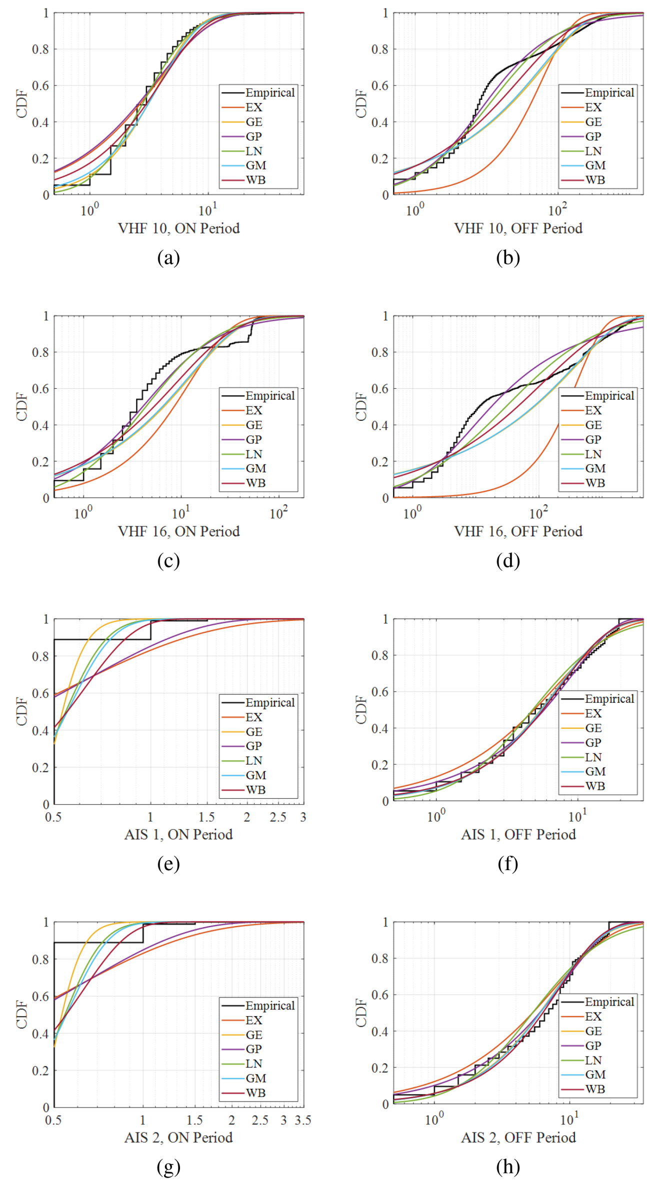

Fig. 9. Fitting results of the four active channels.

A. Definition of Scenario Characteristics

We adopt the ship density computation described in [38]. All AIS ship trajectories are resampled at fixed time interval. For the i-th ship, $S_i = \{s_{i,k}\}_{k=1}^{K}$ denote the set of resampled line segments, where consecutive samples are connected into a segment $s_{i,k} : (\mathbf{p}_{i,k}^0, t_{i,k}^0) \to (\mathbf{p}_{i,k}^1, t_{i,k}^1)$, with length $L_{i,k} = \|\mathbf{p}_{i,k}^1 - \mathbf{p}_{i,k}^0\|$ and duration $\tau_{i,k} = t_{i,k}^1 - t_{i,k}^0$. Here, $\mathbf{p}_{i,k}^{0/1}$ are the start and end coordinates of the segment, and $t_{i,k}^{0/1}$ are the corresponding timestamps. We consider a grid g of 1 km^2 cells for integral time t. Each segment is first geometrically clipped, retaining only the sub-length falling within $g \bigcap t$, denoted $L_{i,k}^{t,g}$. The time contribution of this segment to grid cell g is then defined as

$$\Delta T_{i,k}^{t,g} = \frac{L_{i,k}^{t,g}}{L_{i,k}} \tau_{i,k}. \tag{7}$$

Summing over all ships and segments yields the ship dwell time in grid cell g during integral time t, which is given by

$$T_t^g = \sum_i \sum_k \Delta T_{i,k}^{t,g}. \tag{8}$$

This quantity represents the total ship dwell time within grid g over interval t, with units h/km^2. Based on this value, the expected number of ship positions (i.e., received reports) can be computed. Dividing the total dwell time within the grid by the resampling interval Δt gives the expected number of ship positions during the period. The ship density within the grid g over the integration time t is defined as

$$D_t^g = T_t^g \times 3600/\Delta t. \tag{9}$$

From this, the average ship density over the target waters can be obtained

$$\bar{D}_t = \frac{\sum_{g=1}^{G} D_t^g}{G}, \tag{10}$$

where G represents the total number of grids. In addition, to quantify the spatial concentration of ship activity, we introduce the busy water ship density $\bar{D}_t^{\text{busy}}$ and the busy water ratio P_t^{busy}. $\bar{D}_t^{\text{busy}}$ denotes the ship density over all busy grids within integration time t, reflecting crowding. P_t^{busy} denotes the proportion of busy grids relative to the number of grids with nonzero ship density within integration time t, reflecting the share of busy waters in the entire area. They are defined as

$$\bar{D}_t^{\text{busy}} = \frac{\sum_{g=1}^{G} D_t^g \cdot I_{(D_t^g \geq \theta)}}{\sum_{g=1}^{G} I_{(D_t^g \geq \theta)}}, \tag{11}$$

$$P_t^{\text{busy}} = \frac{\sum_{g=1}^{G} I_{(D_t^g \geq \theta)}}{\sum_{g=1}^{G} I_{(D_t^g > 0)}}, \tag{12}$$

where θ is the high density threshold set to the 90th percentile of ship density samples over the entire observation period. The formulas first partition the waters into "busy" and "free" grids using θ, through $\bar{D}_t^{\text{busy}}$ and P_t^{busy}, they preserve overall ship scale while separately quantifying the share of ships clustered in high density areas.

B. Spectrum Occupancy Model

1) Scenario-Driven NHPP Model: Assume that call arrivals on VHF 10/16 follow an NHPP, with the counting process $N(t)$, $t \geq 0$. The arrival intensity $\lambda(t)$ is driven by an external scenario characteristic vector $\mathbf{z}(t) = [\, z_1(t), \ldots, z_I(t)\,]^\top$ and is specified via a log-link regression

$$\ln \lambda(t) = \beta_0 + \boldsymbol{\beta}^\top \mathbf{z}(t) = \beta_0 + \sum_{i=1}^{I} \beta_i z_i(t), \tag{13}$$

where β_0 is the intercept and $\boldsymbol{\beta}$ is the coefficient vector to be estimated. Estimation can be performed on training ON/OFF sequences using MLE. Equation (13) ensures that the intensity is positive and establishes an explicit mapping from scenario characteristics such as time of day, ship density/number, and busy water crowding degree to the arrival intensity. The NHPP cumulative intensity is

$$\Lambda(s,t) = \int_s^t \lambda(u) du, 0 \leq s < t. \tag{14}$$

Thus, the count distribution over $[s,t)$ is

$$\Pr[N(t) - N(s) = k] = \frac{\Lambda(s,t)^k}{k!} e^{-\Lambda(s,t)}, k = 0, 1, \ldots \tag{15}$$

Furthermore, introduce a single-server, no-queue, blocking-on-busy service mechanism (M/G/1). Let the per-call service time be the random variable with mean $m_S = \mathbb{E}[S]$. With large samples, the channel load and occupancy rate within a integration time satisfy

$$A(t) = \lambda(t) m_S, y(t) = \frac{A(t)}{1 + A(t)} = \frac{\lambda(t) m_S}{1 + \lambda(t) m_S} \in (0,1), \tag{16}$$

where $A(t)$ increases, the occupancy $y(t)$ tends toward 1. Conversely, for small $A(t)$, $y(t)$ is approximately linear in $A(t)$. To obtain a linear relation between occupancy and the influencing characteristics, apply the logit transformation

$$\text{logit}(y_t) = \ln \frac{y(t)}{1 - y(t)} = \ln A(t) = \ln \lambda(t) + \ln m_S. \tag{17}$$

The above shows that the logit of occupancy equals the log-intensity plus a constant $\ln m_S$, where m_S is estimable. Thus, channel occupancy has a linear relation with $\ln(\lambda(t))$.

2) SD-Model Implementation: For the distribution of ON/OFF durations, the observational data support the following: VHF 10 busy times S follow a LN distribution, and VHF 16 busy times S follow a GP distribution. For convenience, the distributions are given below

$$f_{\text{LN}}(s) = \frac{1}{s \sigma_S \sqrt{2\pi}} \exp\left(-\frac{(\ln s - \mu_S)^2}{2\sigma_S^2} \right), s > 0, \tag{18}$$

$$f_{\text{GP}}(s) = \frac{1}{\sigma_S} \left(1 + \xi_S \frac{s - \mu_S}{\sigma_S} \right)^{-1/\xi_S - 1}$$
$$, s \geq \mu_S \text{ and } \left(1 + \xi_S \frac{s - \mu_S}{\sigma_S} \right) > 0. \tag{19}$$

From (13)–(19), the SD-model procedure can be constructed as shown in Algorithm 1.

In summary, we first fit the model on the collected data, and using MLE, perform a linear regression for the NHPP arrival intensity to obtain the regression coefficient vector $\boldsymbol{\beta}$ of the scenario characteristics, while introducing the M/G/1 occupancy mechanism to describe channel usage. Finally, we provide the PDF of the ON time distributions for VHF 10/16 and present pseudocode for the SD-model. In the next section, we analyze the correlation between scenario characteristics and channel occupancy rate, and using the validation set, we compare occupancy fitting accuracy and the complementary cumulative distribution function (CCDF) of ON/OFF times between observed and SD-model to assess the model's agreement with real measurements.

V. Simulation Results and Analysis

In this section, we first use SPSS Statistics 27 to analyze the correlations between the scenario characteristics and channel occupancy rate, so as to identify the scenario characteristics that significantly affect the channel load. We then apply multiple linear regression to estimate the coefficients in (13), and use Algorithm 1 to build the proposed SD-model. Finally, we validate the reliability of the theoretical model by comparing the real-time measurements with the theoretically generated channel state time series. The total observation period of the collected data is 7 days (around 180 hours). The first 90 hours are used as

Algorithm 1: SD-Model for Maritime VHF RT Channels.

Inputs: Integration time t; full observation time T.
Inputs: Scenario-characteristic vector $\mathbf{z}(t)$.
Inputs: Arrival intensity $\lambda(t)$ (see (13)); cumulative intensity $\Lambda(t)$ (see (14)).
Inputs: Busy-time distribution $f_S(\cdot)$ (see (18)/ (19)).
Outputs: Binary occupancy process $X(u) \in \{0,1\},\ u \in [1,T]$.

```
Define B/I denote busy/idle segments.
Initialize B/I ← ∅.
for t = 1 to (T − 1) do
    Compute Λ(t) ← ∫_t^{t+1} λ(u) du        (cf. (14))
    Sample K_t ∼ Poisson(Λ(t))
    Draw K_t trial arrival times {τ_{t,j}}_{j=1}^{K_t} ⊂ (t, t+1];
    sort to obtain τ_{t,1} < ··· < τ_{t,K_t} (NHPP conditional uniformity)
    for j = 1 to K_t do
        Using (18) or (19) to sample busy time S_{t,j} ∼ f_S(·).
        Form the busy segment subset B_{t,j} ← [τ_{t,j}, τ_{t,j} + S_{t,j}].
    end for
    Form the busy segment B_t ← B_{t,1}, B_{t,2}, ..., B_{t,K_t}
    Form the idle segment I_t ← (t, t+1] \ B_t
end for
After loop: define the binary process
X(u) = 1 ← B, X(u) = 0 ← I,   u ∈ [1, T].
return X(u).
```

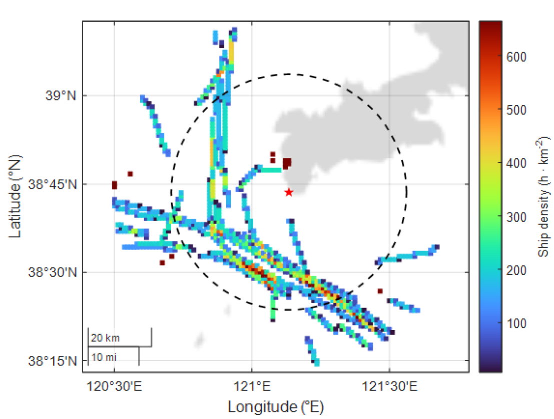

Fig. 10. Ship density thermogram on June 12, 2025, from 6:00 PM to 7:00 PM (local time).

the training set for MLE with the regression coefficient matrix as (13) and the remaining 90 hours form the test set.

Fig. 10 illustrates the ship density heatmap within a 30 nautical miles radius centered on the measurement site. As shown in Fig. 10, the distribution of ship density closely matches the ship tracks of Fig. 6. Most tracks and /high density areas lie within the Laotieshan VTS area designated traffic lanes with high density grids near the port, which visually show the validity of our scenario characteristic definitions. Note that, only grids within 20 nautical miles of the measurement site are considered for (10)–(12). Because the grids within the reporting lines constitute the main area under VTS control, we use this region as the basis for computing the scenario characteristic in Section IV-A.

TABLE IV
FITTING RESULTS FOR VHF 10 OCCUPANCY RATE

	Coefficient	Std. Error	t-value	P-value	VIF
Intercept	.120	.020	6.023	**<.001**	
$\sin_t$	-.163	.003	-2.233	**.027**	1.119
$\cos_t$	-.343	.003	-4.775	**<.001**	1.087
$\bar{D}_t$	.608	.000	2.976	**.003**	8.782
$\bar{D}_t^{\text{busy}}$	-.498	.000	-3.401	**<.001**	4.513
P_t^{busy}	-.240	.079	-1.683	.094	4.265
N_t	.140	.000	1.761	.080	1.324

TABLE V
FITTING RESULTS FOR VHF 16 OCCUPANCY RATE

	Coefficient	Std. Error	t-value	P-value	VIF
Intercept	.030	.006	5.092	**<.001**	
$\sin_t$	-.052	.002	-.675	.500	1.122
$\cos_t$	-.065	.002	-.860	.391	1.074
$\bar{D}_t$	-.356	.000	-2.431	**.016**	4.054
$\bar{D}_t^{\text{line}}$	.119	.000	1.398	.164	1.379
P_t^{busy}	.124	.049	.853	.395	3.978
N_t	.185	.000	2.172	**.031**	1.365

A. Correlation Analysis of Scenario Factors

Tables IV and V present the correlation results for VHF 10 and VHF 16, respectively. The scenario characteristics are considered explanatory variables, and channel occupancy is treated as the dependent variable. The six scenario characteristics are defined as follows: we encode time with $\sin_t = \sin(2\pi t/24)$ and $\cos_t = \cos(2\pi t/24)$, where t denotes the hour index. $\bar{D}_t$ denotes the ship density, $\bar{D}_t^{\text{line}}$ denotes the line-crossing ship density, $\bar{D}_t^{\text{busy}}$ denotes the busy water ship density, P_t^{busy} denotes the busy water ratio, and N_t is the ship number. Using SPSS Statistics 27, we construct a straightforward multiple linear regression and analyze the correlation between the scenario characteristics and channel occupancy. We further use the P-value to assess the contribution of each variable, the adjusted $\bar{R}^2$ to evaluate explanatory power for multiple regressors, the variance inflation factor (VIF) to diagnose multicollinearity, and the Durbin-Watson (DW) statistic to test residual independence.

About VHF 10, the overall explanatory power of the scenario characteristics yields an adjusted $\bar{R}^2 = 16.9\%$, and DW $= 1.4$, indicating slight positive autocorrelation of the residuals. As shown in Table IV, for the temporal components, $\sin_t$ and $\cos_t$ are significant association, indicating intraday periodicity in occupancy. For the spatial characteristics, $\bar{D}_t$ is significantly positively correlated with occupancy, consistent with the qualitative expectation that higher ship density implies busier VHF 10. $\bar{D}_t^{\text{busy}}$ shows a significant association with a negative coefficient. P_t^{busy} and N_t exhibit weak correlations. Collinearity diagnostics indicate $\bar{D}_t$ has the largest VIF, with a value of 8.782, while the

TABLE VI
SCENARIO VECTOR REGRESSION COEFFICIENTS

	β_0	$\sin_t$	$\cos_t$	$\bar{D}_t$	$\bar{D}_t^{\text{line}}$	$\bar{D}_t^{\text{busy}}$	P_t^{busy}	N_t
VHF 10	-4.109	-0.176	-0.195	0.336	$\times$	-0.32	-0.086	0.142
VHF 16	-5.997	-0.324	0.003	-0.234	-0.122	$\times$	0.3	0.212

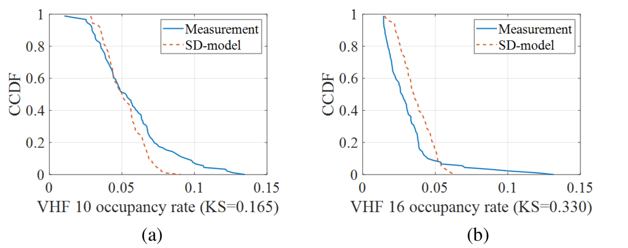

Fig. 11. CCDF comparison of VHF 10/16 occupancy. (a) CCDF comparison of VHF 10 occupancy. (b) CCDF comparison of VHF 16 occupancy.

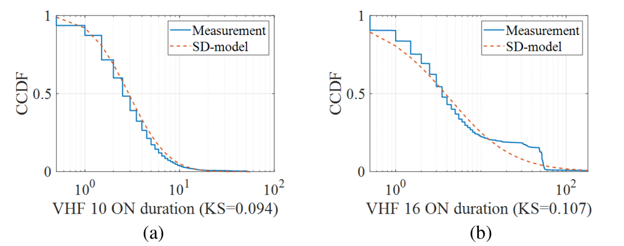

Fig. 12. CCDF comparison of VHF 10/16 ON durations. (a) CCDF comparison of VHF 10 ON duration. (b) CCDF comparison of VHF 16 ON duration.

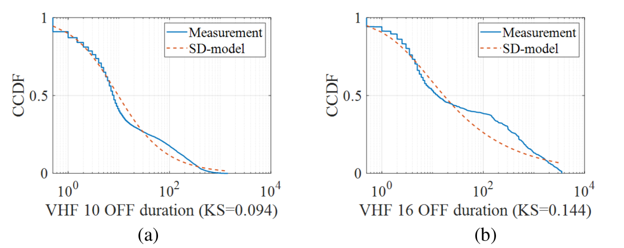

Fig. 13. CCDF comparison of VHF 10/16 OFF durations. (a) CCDF comparison of VHF 10 OFF duration. (b) CCDF comparison of VHF 16 OFF duration.

VIF values of the other characteristics are below 5 and thus within an acceptable range.

About VHF 16, the overall explanatory power yields an adjusted $\bar{R}^2 = 7.3\%$, with DW $= 1.391$, the residuals also exhibit mild positive autocorrelation. As shown in Table V, the two temporal periodic terms are not significant, indicating that VHF 16 occupancy does not exhibit a stable diurnal cycle. Regarding spatial characteristics, $\bar{D}_t$ is significantly negatively correlated and N_t is significantly positively correlated, while the remaining variables are not significant at the 5% level. This result can be interpreted as follows: in waters with higher ship density and intensive traffic, voice interactions are more likely to be conducted with VTS on VHF 10, whereas VHF 16 serves primarily as a broadcast/listening-watch channel, leading to lower occupancy. However, when the overall number of ships in the region increases, broadcast and ad hoc calling raise VHF 16 occupancy, consistent with the *Dalian VTS User Guide* [32] provisions on VHF RT channel usage. All characteristics have VIF values below 5, indicating that multicollinearity is not a concern and the characteristics can be treated as approximately independent.

B. Performance Evaluation of the SD-Model

Fig. 11 shows the CCDF comparison of VHF 10/16 occupancy indicates that the model curve for VHF 10 generally fits the measured curve, but decays faster in the right tail, reflecting a conservative prediction of high intensity periods. For VHF 16, the two CCDF curves coincide almost perfectly over most of the range, yet similarly converge slightly too quickly, underestimating high occupancy periods. The KS distances for VHF 10 and VHF 16 occupancy are approximately 0.165 and 0.33, respectively, indicating good predictive performance.

Fig. 12 shows the CCDFs of VHF 10/16 ON durations. The fits are nearly perfect, with only minor deviations for a few burst events on VHF 16. The corresponding KS values are 0.094 and 0.107, indicating that the generated ON state duration distributions adequately match the measurements. As shown in Fig. 13, a similar observation applies for OFF durations. Predicting OFF state durations is crucial for the generative model, as it determines when secondary user can opportunistically access the channel. The generated OFF state durations for VHF 10/16 exhibit localized mismatches due to the burstiness of VHF RT channel activity, but overall the curves maintain stable average trends. The corresponding KS values are 0.094 and 0.144, indicating high quality prediction of OFF state duration distributions. In summary, the proposed channel occupancy model effectively achieves accurate fitting of occupancy. To facilitate reproducibility, the regression coefficients of the scenario characteristic vector in (13) are provided in Table VI.

VI. CONCLUSION

In this paper, we have conducted a continuous seven-day measurement of maritime VHF band in the near-shore waters of Laotieshan, Dalian, and found out the low overall utilization under current VHF RT/AIS coexistence, indicating substantial spectrum reuse potential. We have further defined a set of scenario characteristics and quantified their effects via correlation analysis. We use an NHPP framework combined with multiple linear regression to relate the scenario characteristics to the arrival rate, proposing a SD-model for maritime VHF RT channels. This paper systematically evaluates the spectrum availability of the maritime VHF band in the Laotieshan waters. VHF 10/16 are VTS designated voice calling channels in this area and support essential maritime communications, including port scheduling, traffic management, and collision avoidance alerts. The measurement findings and modeling methodology presented in this work can be generalized to other VTS designated calling channels with similar functions, offering clear reference value and practical engineering significance. Future work will build on measurement data and theoretical models, and leverage the proposed SD-model to further investigate cognitive radio techniques such as spectrum sensing, spectrum prediction, and dynamic spectrum access, enabling the broadband maritime digital communications.

References

[1] *Technical Characteristics for a VHF Data Exchange System in the VHF Maritime Mobile Band*, Rec. ITU-R M.2092-1, International Telecommunications Union, Geneva, Switzerland, Feb. 2022.

[2] International Association of Marine Aids to Navigation and Lighthouse Authorities (IALA), "Maritime radio communications plan (MRCP)" IALA, Saint-Germain-en-Laye, France, Tech. Rep., Dec. 2017. [Online]. Available: https://www.iala.int/product/maritime-radio-communications-plan/

[3] X. Hu, B. Lin, P. Wang, H. Lyu, and T.-S. Li, "A collision feedback based multiple access control protocol for very high frequency data exchange system in E-navigation," *J. Navigation*, vol. 74, no. 4, pp. 822–837, 2021.

[4] Y. Mi et al., "Measurement-based characterization and modeling of land-to-ship wireless channels at 3.2 GHz," *IEEE Trans. Antennas Propag.*, vol. 73, no. 1, pp. 441–452, Jan. 2025.

[5] Y. Lyu et al., "An experimental analysis and modeling of short term fading channel for beyond horizon maritime communications at 25 GHz in South China sea," *IEEE Antennas Wireless Propag. Lett.*, vol. 23, no. 12, pp. 4468–4472, Dec. 2024.

[6] Q. Zhang, S. Wang, Y. Shi, and K. Yang, "Measurements and analysis of maritime wireless channel at 8 GHz in the south China sea region," *IEEE Trans. Antennas Propag.*, vol. 71, no. 3, pp. 2674–2681, Mar. 2023.

[7] B. Yamamoto et al., "Received signal strength indication (RSSI) of 2.4 GHz and 5 GHz wireless local area network systems projected over land and sea for near-shore maritime robot operations," *J. Mar. Sci. Eng.*, vol. 7, no. 9, 2019, Art. no. 290.

[8] F. Li, Y. Shui, J. Liang, K. Yang, and J. Yu, "Ship-to-ship maritime wireless channel modeling under various sea state conditions based on REL model," *Front. Mar. Sci.*, vol. 10, 2023, Art. no. 1134286.

[9] W. Wang, T. Jost, and R. Raulefs, "A semi-deterministic path loss model for in-harbor LoS and NLoS environment," *IEEE Trans. Antennas Propag.*, vol. 65, no. 12, pp. 7399–7404, Dec. 2017.

[10] J.-H. Lee, J. Choi, W.-H. Lee, J.-W. Choi, and S.-C. Kim, "Measurement and analysis on land-to-ship offshore wireless channel in 2.4 GHz," *IEEE Wireless Commun. Lett.*, vol. 6, no. 2, pp. 222–225, Apr. 2017.

[11] L. Yee Hui, F. Dong, and Y. S. Meng, "Near sea-surface mobile radiowave propagation at 5 GHz: Measurements and modeling," *Radioengineering*, vol. 23, no. 3, pp. 824–830, 2014.

[12] A. Constantinides, H. Haralambous, H. Papadopoulos, and M. Makrominas, "Models of HF interference over Cyprus," *Appl. Sci.*, vol. 12, no. 22, 2022, Art. no. 11808.

[13] H. Haralambous and H. Papadopoulos, "24-h HF spectral occupancy characteristics and neural network modeling over northern Europe," *IEEE Trans. Electromagn. Compat.*, vol. 59, no. 6, pp. 1817–1825, Dec. 2017.

[14] M. G. Mostafa, E. Tsolaki, and H. Haralambous, "HF spectral occupancy time series models over the eastern mediterranean region," *IEEE Trans. Electromagn. Compat.*, vol. 59, no. 1, pp. 240–248, Feb. 2017.

[15] S. D. Barnes, P. R. Botha, and B. Maharaj, "Spectral occupation of tv broadcast bands: Measurement and analysis," *Measurement*, vol. 93, pp. 272–277, 2016.

[16] D. Corral-De-Witt, S. Ahmed, F. Awin, J. L. Rojo-Álvarez, and K. Tepe, "An accurate probabilistic model for TVWS identification," *Appl. Sci.*, vol. 9, no. 20, 2019, Art. no. 4232.

[17] H. Rutagemwa, K. E. Baddour, and A. Ghasemi, "Spectrum sharing opportunities in land mobile radio bands: A data-driven approach," in *Proc. 2017 IEEE 28th Annu. Int. Symp. Personal, Indoor, Mobile Radio Commun.*, 2017, pp. 1–5.

[18] M. López-Benıtéz and F. Casadevall, "Empirical time-dimension model of spectrum use based on a discrete-time Markov chain with deterministic and stochastic duty cycle models," *IEEE Trans. Veh. Technol.*, vol. 60, no. 6, pp. 2519–2533, Jul. 2011.

[19] M. López-Benıtéz and F. Casadevall, "Time-dimension models of spectrum usage for the analysis, design, and simulation of cognitive radio networks," *IEEE Trans. Veh. Technol.*, vol. 62, no. 5, pp. 2091–2104, Jun. 2013.

[20] M. López-Benıtéz and F. Casadevall, "Space-dimension models of spectrum usage for cognitive radio networks," *IEEE Trans. Veh. Technol.*, vol. 66, no. 1, pp. 306–320, Jan. 2017.

[21] A. Palaios, J. Riihijärvi, O. Holland, and P. Maehoenen, "Detailed measurement study of spatial similarity in spectrum use in dense urban environments," *IEEE Trans. Veh. Technol.*, vol. 66, no. 10, pp. 8951–8963, Oct. 2017.

[22] L. Wang, J. Hu, C. Zhang, R. Jiang, and Z. Chen, "Deep learning models for spectrum prediction: A review," *IEEE Sensors J.*, vol. 24, no. 18, pp. 28553–28575, Sep. 2024.

[23] Y. Chen and H.-S. Oh, "A survey of measurement-based spectrum occupancy modeling for cognitive radios," *IEEE Commun. Surv. Tut.*, vol. 18, no. 1, pp. 848–859, First quarter 2016.

[24] M. Höyhtyä et al., "Spectrum occupancy measurements: A survey and use of interference maps," *IEEE Commun. Surv. Tut.*, vol. 18, no. 4, pp. 2386–2414, Fourth quarter 2016.

[25] D. Das and S. Das, "A survey on spectrum occupancy measurement for cognitive radio," *Wireless Pers. Commun.*, vol. 85, no. 4, pp. 2581–2598, 2015.

[26] D. Datla, A. M. Wyglinski, and G. J. Minden, "A spectrum surveying framework for dynamic spectrum access networks," *IEEE Trans. Veh. Technol.*, vol. 58, no. 8, pp. 4158–4168, Oct. 2009.

[27] F. Azmat, Y. Chen, and N. Stocks, "Analysis of spectrum occupancy using machine learning algorithms," *IEEE Trans. Veh. Technol.*, vol. 65, no. 9, pp. 6853–6860, Sep. 2016.

[28] S. Li et al., "A novel multi-scale time fusion transformer for long-range spectrum occupancy prediction," *IEEE Trans. Veh. Technol.*, vol. 74, no. 6, pp. 9299–9312, Jun. 2025.

[29] Y. Hu, Q. Chen, S. Zhuo, R. Fan, and X. Ding, "Feasibility study on improving the frequency utilization for VHF COM in airport terminal area," in *Proc. 2020 IEEE 2nd Int. Conf. Civil Aviation Saf. Inf. Technol.*, 2020, pp. 1126–1131.

[30] R. T. Loquias, C. A. G. Hilario, M. F. D. De Guzman, and J. J. S. Marciano, "Quantitative assessment of TV white space in the western Philippine nautical highway," in *Proc. 2019 IEEE Int. Symp. Dynamic Spectr. Access Netw.*, 2019, pp. 1–8.

[31] H. E. A. Elshafie et al., "VHF band utilization measurement for cognitive radio application in Malaysia," *Wireless Pers. Commun.*, vol. 85, no. 4, pp. 2727–2747, 2015.

[32] Dalian maritime safety administration of China and Dalian vessel traffic service center, "Dalian VTS guide for users (3rd edition)," PDF, Jan. 2013. Accessed: Dec. 23, 2025. [Online]. Available: https://www.piclub.or.jp/wp-content/uploads/2013/01/1262.pdf

[33] *Methods for Measurements of Radio Noise*, ITU-R SM.1753-2, International Telecommunication Union (ITU), Geneva, Switzerland, Sep. 2012.

[34] L. Falco, A. Pititto, W. Adnams, N. Earwaker, and H. Greidanus, "EU Vessel Density Map: Detailed method," Publications Office of the European Union, Luxembourg, Technical report, Nov. 2023, doi: 10.2771/518143.

[35] M. Wellens, J. Riihijärvi, and P. Mähönen, "Empirical time and frequency domain models of spectrum use," *Phys. Commun.*, vol. 2, no. 1/2, pp. 10–32, 2009.

[36] W. H. Press, *Numerical Recipes 3rd Edition: The Art of Scientific Computing*. Cambridge, U.K.: Cambridge Univ. Press, 2007.

[37] A. Bhattacharyya, "On a measure of divergence between two statistical populations defined by their probability distribution," *Bull. Calcutta Math. Soc.*, vol. 35, pp. 99–110, 1943.

[38] L. Falco, A. Pititto, W. Adnams, N. Earwaker, and H. Greidanus, "Eu vessel density map: Detailed method (v1.6)," *European Commission, Directorate-General for Maritime Affairs and Fisheries (DG MARE)*, EMODnet, Luxembourg, Nov. 2023.

Chensong Zhao received the B.S. degree in communication engineering from Dalian Jiao Tong University, Dalian, China, in 2019, and the M.S. degree in information and communication engineering from Dalian Maritime University, Dalian, China, in 2022. He is currently working toward the doctoral degree with the School of Information Science and Technology, Dalian Maritime University, Dalian. His research interests include cognitive radio, machine learning, and maritime communication.

Qing Hu received the Ph.D. degree in communication and information system from Dalian Maritime University, Dalian, China, in 2011. He is currently a Professor with the School of Information Science and Technology, Dalian Maritime University. His research interests include maritime communication, e-Navigation, the Internet of Ship (IoV), automatic identification system, and very high frequency (VHF) data exchange system.

Yanpeng Dai (Member, IEEE) received the B.Eng. degree from Shandong Normal University, Jinan, China, in 2014, and the Ph.D. degree from Xidian University, Xi'an, China, in 2020. He was a Visiting Student at the University of Waterloo, Waterloo, ON, Canada. He is currently an Associate Professor with the School of Information Science and Technology, Dalian Maritime University, Dalian, China. His research interests include resource management and interference coordination for heterogeneous wireless networks and maritime networking.

Chang Liu received the M.E. and Ph.D. degrees in communication and information system from Dalian Maritime University, Dalian, China. She is currently an Associate Professor with Electronic and Information Department, Information Science and Technology College, Dalian Maritime University. Her research interests include maritime intelligent communication, vessel automatic identification system, radar signal processing, and multi-sensor fusion.

Shuaiheng Huai (Member, IEEE) received the B.E. degree from the Beijing University of Posts and Telecommunications, Beijing, China, in 2011, the M.Sc. degree from the University of Edinburgh, Edinburgh, U.K., in 2012, and the Ph.D degree from Dalian Maritime University, Dalian, China, in 2020. He is currently an Assistant Professor with the School of Information Science and Technology, Dalian Maritime University. His research interests include localization and navigation application technology, and maritime communication technology.

Nan Cheng (Senior Member, IEEE) received the B.E. and M.S. degrees from the Department of Electronics and Information Engineering, Tongji University, Shanghai, China, in 2009 and 2012, respectively, and the Ph.D. degree from the Department of Electrical and Computer Engineering, University of Waterloo, Waterloo, ON, Canada, in 2016. From 2017 to 2019, he was a Postdoctoral Fellow with the Department of Electrical and Computer Engineering, University of Toronto, Toronto, ON. He is currently a Professor with the State Key Laboratory of ISN and the School of Telecommunications Engineering, Xidian University, Xi'an, China. He has authored or coauthored more than 90 journal papers in IEEE TRANSACTIONS and other top journals. His research interests include B5G/6G, AI-driven future networks, and space–air–ground integrated networks. He is the Editor/Associate Editor for IEEE TRANSACTIONS ON VEHICULAR TECHNOLOGY, IEEE OPEN JOURNAL OF THE COMMUNICATIONS SOCIETY, and *Peer-to-Peer Networking and Applications*. He is/was the Guest Editor of several journals.

Xuemin (Sherman) Shen (Fellow, IEEE) received the Ph.D. degree in electrical engineering from Rutgers University, New Brunswick, NJ, USA, in 1990. He is currently a University Professor with the Department of Electrical and Computer Engineering, University of Waterloo, Waterloo, ON, Canada. His research interests include network resource management, wireless network security, the Internet of Things, 5G and beyond, and vehicular networks. He is a registered Professional Engineer of Ontario, Canada, Engineering Institute of Canada Fellow, Canadian Academy of Engineering Fellow, Royal Society of Canada Fellow, Chinese Academy of Engineering Foreign Member, and International Fellow of the Engineering Academy of Japan. He was the recipient of the "West Lake Friendship Award" from Zhejiang Province in 2023, President's Excellence in Research from the University of Waterloo in 2022, Canadian Award for Telecommunications Research from Canadian Society of Information Theory (CSIT) in 2021, R. A. Fessenden Award from IEEE, Canada, in 2019, Award of Merit from the Federation of Chinese Canadian Professionals (Ontario) in 2019, James Evans Avant Garde Award from the IEEE Vehicular Technology Society in 2018, Joseph LoCicero Award in 2015 and Education Award in 2017 from the IEEE Communications Society (ComSoc), and Technical Recognition Award from the Wireless Communications Technical Committee in 2019 and AHSN Technical Committee in 2013. He has also recipient of the Excellent Graduate Supervision Award from the University of Waterloo in 2006 and the Premier's Research Excellence Award (PREA) from the Province of Ontario, Canada, in 2003. He serves/served as the General Chair of the 6G Global Conference 2023 and ACM Mobihoc 2015, Technical Program Committee Chair/Co-Chair for IEEE Globecom 2024, 2016, and 2007, IEEE Infocom 2014, and IEEE VTC 2010 Fall, and Chair of IEEE ComSoc Technical Committee on Wireless Communications. He is the Past President of the IEEE ComSoc, Vice President of Technical and Educational Activities, Vice President of Publications, Member-at-Large on the Board of Governors, Chair of the Distinguished Lecturer Selection Committee, and member of the IEEE Fellow Selection Committee of the ComSoc. He served as the Editor-in-Chief of IEEE INTERNET OF THINGS JOURNAL, IEEE NETWORK, and *Peer-to-Peer Networking and Applications*.